Construction and Building Materials 371 (2023) 130765

Contents lists available at ScienceDirect

Construction and Building Materials

journal homepage: www.elsevier.com/locate/conbuildmat

Early hydration of belite-ye'elimite-ferrite cements: Role of admixtures

Raquel Pérez-Bravo, Alejandro Morales-Cantero, Ana Cuesta, Miguel A.G. Aranda, Isabel Santacruz, Angeles G. De la Torre *

Departamento de Química Inorgánica, Cristalografía y Mineralogía, Universidad de Málaga, Málaga 29071, Spain

ARTICLE INFO

Keywords:
CO_2 footprint
$CaCl_2$
TIPA
Rietveld analysis
Synchrotron radiation

ABSTRACT

The effect of TIPA and $CaCl_2$ on early hydration, i.e. 24 h, of a B-BYF cement has been studied by *in situ* synchrotron X-ray powder diffraction, calorimetry, thermal analysis, NMR, and rheological measurements of the pastes and mechanical strength of the corresponding mortars. The addition of 0.05 %*bwc (by* weight of cement*)* of TIPA reduced the viscosity of the paste during the first minutes of hydration but, after the end of the induction period, ~7 h, it favored the formation of AFt compared to the reference paste. The latter is likely due to the acceleration of the dissolution of the amorphous aluminates and sulfates by the presence of TIPA. These results correlate with the increase of ~169% of the 1-day mechanical strengths. The addition of 2.0 %*bwc* of $CaCl_2$ accelerated the dissolution rate of ye'elimite, causing an increase of the amount of precipitated ettringite even before the end of the induction period, which has been shorted to ~6 h. The 1-day mechanical strengths of the mortars with this admixture outperforms that of the reference mortar by 181%. Finally, ferrite and α_H-belite reactivities were not affected by the addition of any of these admixtures during the first 24 h of hydration of this cement.

1. Introduction

There is an undoubted impact on climate change linked to the Portland cement production [1], with an estimation of ~0.87 tons of CO_2 per ton of manufactured clinker Portland, considering the decarbonation of raw materials and fuel consumption in the kilns. Considering these values, and the PC global production of more than 4 Gt in 2022 [2], the estimated contribution of cement sector to global climate change is ~8% [3]. Belite-Ye'elimite-Ferrite (BYF) cements are low-carbon materials due to their lower need of calcium in the raw material and the lower temperature of production [4]. Their main phases (in order of abundance) of the BYF clinkers are dicalcium silicate, belite (C_2S), and Klein salt or ye'elimite, $C_4A_3\,\overline{S}$ [5]. The reactivity of these cements depends on the composition of the clinker and on the type and amount of calcium sulfate added [6,7], but the main hydration product at early ages is the formation of crystalline ettringite and nanocrystalline hydrated aluminum hydroxide [8] due to the reaction of ye'elimite with anhydrite and water, reaction (1), in cement nomenclature [CaO = C; SiO_2 = S; Al_2O_3 = A; SO_3=$\overline{S}$; H_2O = H; Fe_2O_3 = F]:

$$C_4A_3\overline{S} + 2C\,\overline{S} + 38H \rightarrow C_6A\,\overline{S}_3H_{32} + 2AH_3{\cdot}5H \quad (1)$$

Depending on the amount of sulfate, other phases such as AFm, $C_4A\,\overline{S}\,H_{12}$, may precipitate at early ages. These reactions usually occur within the first 24 h and most of the heat evolved is due to these reactions.

Reactions related to ye'elimite and the formation of ettringite are very fast, causing rapid setting and strength development but at the same time they present a loss of fluidity at early ages and poor workability, that pushes these cements into niche applications [9,10]. This fact is caused by the strong dependence of the final performances on the composition of this ye'elimite based cements. For instance, the ye'elimite/soluble sulfate ratio close to that of reaction (1), yields to high early strength mortars. Besides, these systems can be used as repairing materials due to their self-leveling properties if ettringite is formed by a different pathway in which calcium hydroxide is present [11]. Moreover, it is highly advisable to use superplasticizers [12], to maintain their initial fluidity, and retarders [13–15], when needed, to counteract the loss of dispersion efficiency of superplasticizers due to their high reactivity, in order to use them in larger-scale applications.

Belite reactivity is much slower than ye'elimite, and the formation of stratlingite, C_2ASH_8, and AFm type phase, can be expressed by reaction (2), which comprises its reactivity with aluminates [16]:

$$C_2S + AH_3 + 5H \rightarrow C_2ASH_8 \quad (2)$$

* Corresponding author.
E-mail address: mgd@uma.es (A.G. De la Torre).

https://doi.org/10.1016/j.conbuildmat.2023.130765
Received 21 November 2022; Received in revised form 14 February 2023; Accepted 15 February 2023

Since the reactivity of belite is slow, in order to make these cements competitive to PC, some attempts have been performed to increase their reactivity: i) by adding stabilizers of α-forms of belite in the clinkering step, as they are more reactive polymorphs [16–18], or ii) by preparing BYF but with a small amount of alite in their composition, to profit from the higher reactivity at early ages of this phase[19–21]. All these attempts have yielded to materials with enhanced mechanical strengths. Complementary to these strategies, the use of certain accelerators may be a way to increase belite reactivity and finally, to enhance mechanical strengths. $CaCl_2$ has been used as an accelerator of PC, especially to be used to counteract the effect of low temperatures. The effects of this admixture on hydration kinetic have been extensively studied [22], and there are some hypotheses about the effect on C_3S, aluminates and sulfates dissolution or C-S-H resulting microstructure. However, this admixture has to be used with caution because chloride ions are able to depassivate the surface of steel, by forming soluble chlorides, breaking the protective oxide layer produced at the high pH of cement paste [23]. In cements based on calcium sulfoaluminate, the use of inorganic admixtures to accelerate the rate of hydration at low temperatures has been described [24]; although these authors point out the enhancement of belite reactivity by inorganic accelerators, they do not use $CaCl_2$. Other family of accelerators are alkanolamines, such as triethanolamine (TEA) or triisopropanolamine (TIPA) which have been recently used to minimize the retarding effect of superplasticizers in PC [25], or as a strength-enhancing agent in high C_4AF cements [26].

In this work, an activated BYF cement, containing stabilized α'_H-belite by the addition of borax at the clinkering step [27], has been hydrated in the presence of superplasticizers jointly with $CaCl_2$ or TIPA. A synchrotron X-ray powder diffraction study during the first 24 h of hydration has been performed to unravel the effect of admixtures on the hydration kinetic of this cement. Moreover, these results in combination with those obtained by ^{27}Al MAS-NMR, calorimetry, rheology and thermogravimetric analysis, have been correlated with the mechanical strengths at 1 day of hydration.

2. Materials and methods

2.1. Materials

2 kg of BYF clinker were synthesized in the laboratory with the addition of B_2O_3 in the form of borax (to stabilize α'_H-C_2S). This clinker was prepared following the procedure reported elsewhere [27]. Briefly, the raw materials to prepared the clinker were pre-homogenized in a micro-Deval machine with steel balls. Next, the raw mixture was placed in a crucible Pt/Rh pressed as pellets (ϕ = 55 cm × 5 cm height). The pellets were clinkered by following a heating ramp with five segments: 1) from room temperature to 900 °C at 5 °C/min; 2) holding for 30 min; 3) from 900 to 1350 °C at 5 °C/min; 4) holding for 30 min; and 5) quenching. Finally, the clinker was ground. Then, the cement was prepared by milling the clinker with 10 wt% of anhydrite to prepare the cements up to a Blaine parameter of 526 m^2/kg. Table 1 gives the elemental composition determined by XRF and phase assemblage of the B-BYF_REF cement determined by SXRPD and Rietveld method, as detailed elsewhere [27] (including the Amorphous and Crystalline non-quantified, ACn) see below.

A commercial polycarboxylate-based superplasticiser (SP), with 25 wt% of active matter (Floadis 1623 marketed by Adex Polymer S.L., Madrid, Spain), was used to assure the flowability of the pastes and mortars. As accelerators, two commercially available admixtures were used: Triisopropanolamine, TIPA, 98% from Acros Organics, and $CaCl_2$, 96.3%, from Fluka™.

2.2. Paste preparation

The water to cement (w/c) ratio was 0.40 for all the pastes. The selected amount of SP was 0.4 wt%, active matter by weight of cement (*bwc*), which was previously optimised [28]; the water of the SP was considered for w/c ratio. The amounts of admixtures were 0.05 wt% of TIPA and 2.0 %*bwc* $CaCl_2$.

Table 1
Elemental composition, expressed as weigh percentage of oxides, determined by XRF, including loss on ignition (LOI) and mineralogical composition determined by SXRPD and Rietveld method, including ACn content for B-BYF_REF.

Chemical composition from XRF (wt%)		Mineralogical composition from SXRPD (wt%)	
CaO	50.6	α'_H-C_2S	38.1
SiO_2	13.7	$C_4A_3\overline{S}$ [&]	22.2
SO_3	10.4	C_4AF	20.6
Al_2O_3	14.9	C_2AS	0.6
Fe_2O_3	5.4	$C\overline{S}$	9.0
MgO	0.9	ACn	9.5
TiO_2	0.5		
K_2O	0.3		
Na_2O*	0.8		
B_2O_3*	1.8		
LOI	0.7		

* Nominal percentage added as borax.
& Data corresponding to the sum of cub-$C_4A_3\overline{S}$ and ort-$C_4A_3\overline{S}$.

2.3. In situ synchrotron X-Ray powder diffraction (SXRPD) data collection and analysis

Quartz, SiO_2 99.5% (AlfaAesar) was added to the cement powder as internal standard, 12.0 wt%, and mixed manually using an agate mortar, to determine the total amount of amorphous phases of the pastes (Amorphous and Crystalline not-quantified, ACn) [29]. Consequently, the mixture of cement with quartz (Cement-Q) was used to prepare the pastes to perform the *in situ* SXRPD as follow: in all cases, SP was added to water and stirred for 1 min with magnetic stirrer prior to binder addition. Pastes with TIPA or $CaCl_2$, were firstly prepared with w/c of 0.35 with the SP-water and stirred for 1 min, in step 1 of Fig. 1. After that, a dissolution with the accelerator admixture ($admixture_{aq}$ in Fig. 1) was added (in the appropriated proportion to achieve w/c of 0.40 and the desired amount of admixture) and (manually) stirred for 30 s and mixed (with a vortex) for other 30 s, step 2 in Fig. 1. Finally, pastes were injected with a syringe in the borosilicate capillaries (0.7 mm of diameter) and sealed with grease to avoid water loss.

The powder diffraction end station of MSPD-BL04 beamline at ALBA synchrotron (Barcelona, Spain) was used to perform the *in situ* SXRPD study [30] by selecting a wavelength of 0.62005(1) Å (20 keV), and using the MYTHEN detector. The capillaries were rotating at 20 rpm during data collection, which took 6 min per pattern [from 2 to 40° (2θ)]. The temperature at the experimental hutch was 22 ± 1 °C.

The powder patterns were analyzed by using the Rietveld methodology with GSAS-II software [31], with the instrumental parameters determined with the Si SRM 640e standard, and collected in the same conditions [32]. The crystal structures used are those published elsewhere [33,34].

2.4. Calorimetry analysis

An eight-channel Thermal Activity Monitor (TAM Air from TA Instruments) calorimeter was used. Glass ampoules of 20 ml with distilled water were used as reference according to [35], and ampoules with the samples were also inserted in the calorimeter. The studied pastes (~6 g) were prepared in the same way as for the *in situ* SXRPD study, Fig. 1, without quartz; pastes were introduced into the ampoules with a syringe and immediately placed into the calorimeter to start the measurement. The methodology described in [36] was followed to measure calorimetry from the very beginning. The heat flow data were collected at 20 °C

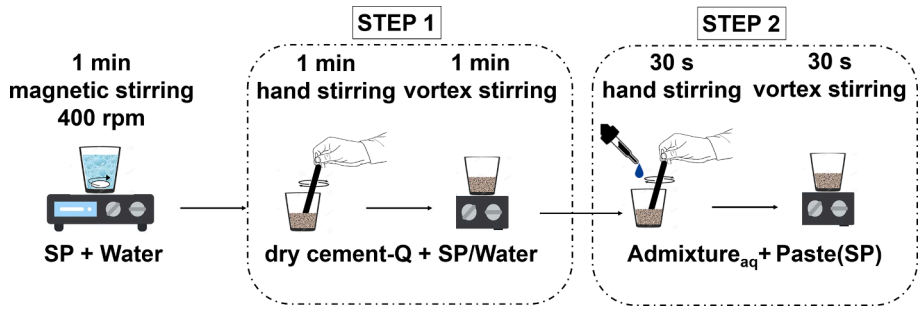

Fig. 1. Sketch of the experimental procedure employed to prepare the pastes.

and are represented per gram of anhydrous cement. Prior to the calorimeter study, all the materials (cement, admixtures and water) were maintained at 20 °C for 24 h.

2.5. ^{27}Al MAS-NMR

For the ^{27}Al MAS-NMR study, the cement-Q pastes were prepared following the same procedure detailed in Fig. 1. The hydration was arrested after 4 and 24 h as detailed in [28,37]. To collect ^{27}Al MAS-NMR spectra, a Bruker AVIII HD 600NMR spectrometer was used, at 156.4 Hz, whose specs are: field strength of 14.1 T and rotors operating at 20 kHz. The experimental conditions are listed below: single pulse (π/12), excitation pulse of 1 μs and 5.0 s relaxation delay and 200 scans. An external solutions $Al(NO_3)_3$ 1 M was used to refer the chemical shifts. The deconvolutions of the spectra have been performed with the DMFIT software. The line shape of the ^{27}Al peaks associated with yéelimite (Al^{IV}) and amorphous phases (Al^{VI}) were described by Czjzek model. For ettringite the peaks associated were described by a lorentzian/gaussian function [38,39].

2.6. Thermogravimetric analysis (TGA)

Pastes (without quartz) with w/c = 0.4 were prepared in cylinders to perform TGA. The anhydrous cement and water + SP, without or with admixture, were mechanically stirred at 800 rpm twice during 90 s with 30 s of pause in between. Finally, 30 s of stirring were applied. Pastes were poured into PTFE molds, hermetically closed and cured at 20 °C rotating in a rolling table during 24 h [40]. The hydration was arrested after 24 h by manually gently grinding and using isopropanol and diethyl ether [28,37]. The samples were stored at 40 °C for 24 h in a stove before performing the thermogravimetric analysis [41]. The stopped-pastes were placed in open platinum crucibles under air flow and heated from room temperature (RT) to 1000 °C (at 10 °C/min) in an SDT-Q600 analyzer from TA instruments. The free water was calculated by using the equations (3) and (4) [20]:

$$BW = \frac{BW_{ATD} \times CEM}{100 - BW_{ATD}} \quad (3)$$

$$FW = TW - BW \quad (4)$$

being BW the chemically bounded water; BW_{ATD} the weight loss measured from RT to 600 °C from DTA-TGA curves; CEM the cement content; and TW the nominal added water, all values in weight percentage.

2.7. Rheological study

Pastes (without quartz) were prepared using the same methodology detailed for TGA. The effect of the accelerator on the rheological behavior of the fresh pastes was studied using a rotational viscometer (VT550, Thermo Scientific Haake, Germany). Pastes (55 ml) were measured in a stainless steel serrated coaxial cylinder sensor (MV2P), provided with a lid to minimize evaporation. Flow curves were measured at controlled rate, from 2 to 350 s^{-1} (up-curve), for a total of 12 ramps (up-curve), with ramp times of 6 s. And from there, following the same ramp times, from 350 to 2 s^{-1}, were measured for the down-curve. Pastes were pre-sheared at 350 s^{-1} (for 30 s) and held at 0 s^{-1} (for 5 s) before the measurement. Data were acquired after 8 min since the cement powder was added to water.

2.8. Mortar preparation

Mortars (3 × 3 × 3 cm^3) were prepared according to UNE-EN-196-1. Mortars were cured at 20 ± 1°C in a humidity chamber at 99% relative humidity (RH) for 24 h, then demolded and tested. A correction factor (1.78) was applied to assure that the given values were comparable to standard prisms (4 × 4 × 16 cm^3) [16]. Mortars were tested in the device located at Málaga Cement factory (Votarantim Cimentos group, Málaga, Spain).

3. Results and discussion

3.1. In situ synchrotron X-ray powder diffraction study

Figs. 2, 3 and 4 show selected SXRPD raw data plots during the first ~24 h of hydration for B-BYF_REF, B-BYF_0.05TIPA and B-BYF_2.0$CaCl_2$ pastes, respectively, as a representative example, to illustrate the changes occurring during this period of time. As a first sight, the main (and only) change in the patterns is the dissolution of ye'elimite and anhydrite, and the crystallization of ettringite, see reaction (1). Diffraction peaks from AFm were not observed at any time during this hydration period.

The enlarged low angle region of the patterns (at the bottom) shows the diffraction peaks of ettringite and C_4AF. Ettringite reflection is increasing with time and ferrite diffraction peak is constant, indicating that the latter is not dissolving within the first ~24 h of hydration. It has been described [26] that TIPA can complex with Fe^{3+} to accelerate the dissolution and hydration of C_4AF in a high-pH slurry. Consequently, the absence of ferrite reactivity can be justified mainly due to the low dosage added [42] jointly with the lower pH of BYF slurries [43].

Fig. 5 shows selected SXRPD raw data plots at selected ranges for the three pastes. The left panels show the main diffraction peaks of ye'elimite (~9.5° ($2\theta_{\lambda=0.62\ Å}$) and anhydrite (~10.2° ($2\theta_{\lambda=0.62\ Å}$), both decreasing in all pastes. With the objective of illustrating the trend of dissolution of ye'elimite and anhydrite, a red dotted line joining the intensity of reflections at ~9.5° and ~10.2° ($2\theta_{\lambda=0.62\ Å}$) in the ~24 h SXRPD pattern has been included. In B-BYF_REF and B-BYF_0.05TIPA pastes, the red dotted line has a negative slope, while in the paste with $CaCl_2$ the slope of this line is positive, indicating a different dissolution/reaction degree of these phases. Specifically, anhydrite is dissolving/reacting at a slower pace. This behavior will be discussed below. The right panels show a range where the main diffraction peaks of α'_H-C_2S are located (arrows in Fig. 5), and are not changing with time, showing that this phase is not dissolving significantly in the first ~24 h.

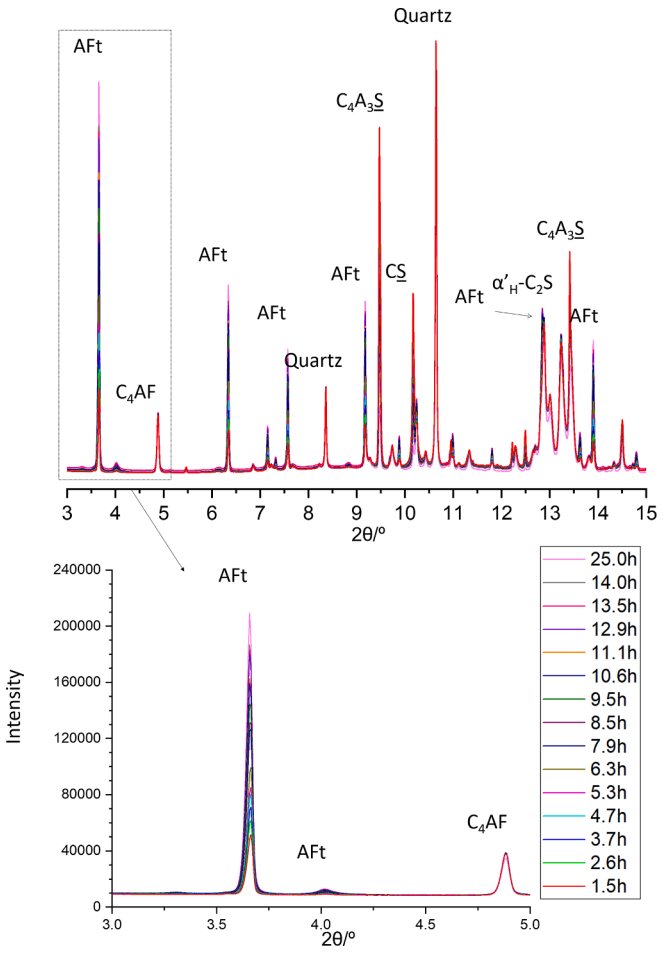

Fig. 2. Selected SXRPD raw patterns (λ = 0.62 Å) for B-BYF_REF paste. Bottom: enlarged low angle region.

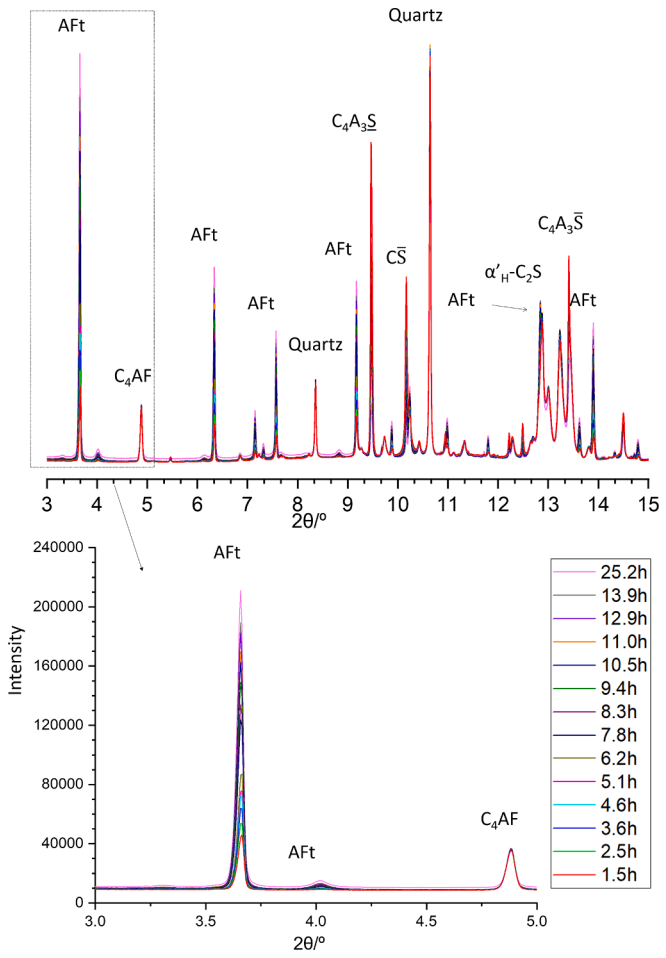

Fig. 3. Selected SXRPD raw patterns (λ = 0.62 Å) for B-BYF_0.05TIPA paste. Bottom: enlarged low angle region.

All the SXRPD patterns were analyzed to obtain the Rietveld Quantitative Phase Analysis (RQPA), including the indirect quantification of ACn, as detailed in the materials and methods section. Fig. S3, as supplementary material, shows the Rietveld plots of the three pastes at selected hydration times, ~1.5, ~10 and 22 h, as representative examples of the goodness of fits at any hydration time. Tables S1 to S3, deposited as supplementary material, give the phase assemblage, including the total ACn content, of the three pastes at all the studied hydration times. It is important to clarify that the ACn_{Total} included in these tables mainly comprises the nanocrystalline/amorphous aluminum hydrates, viz aluminum hydroxide or AFm-related phases, as well as the free water (FW), i.e. the non-chemically bounded water. Under the assumption of certain hydration reaction, that is discussed below, these data have been used to estimate these two components of ACn_{Total}.

Fig. 6 shows the weight percentages as a function of time of ye'elimite, anhydrite and ettringite for the three studied pastes from RQPA. The dissolution/reaction rates of ye'elimite and anhydrite in B-BYF_REF and B-BYF_0.05TIPA are almost coincident, as well as the crystallization of AFt before ~7 h. After this time, slightly more AFt has precipitated in the TIPA-containing paste than in the reference paste. The addition of $CaCl_2$ has accelerated the dissolution of ye'elimite, before ~7 h, meanwhile the dissolution of anhydrite has been partially delayed. It has been previously described that the addition of Ca^{2+} containing salts change the solubility of anhydrite [44], which may justify this behavior. Moreover, the precipitation of AFt follows a slightly different pathway in B-BYF_2.0$CaCl_2$ than in the other two pastes, likely due to the change of solubility of anhydrite. The discussion to understand this behavior is detailed below.

Fig. 7a shows the crystalline anhydrite/ye'elimite molar ratio as a function of time, calculated from RQPA reported in Tables S1 to S3. Considering reaction (1), the stoichiometric C $\overline{S}$/C_4A_3 $\overline{S}$ molar ratio is 2.0, also indicated in Fig. 7a. B-BYF_REF and B-BYF_0.05TIPA results are close to 2.0, especially at 24 h, while B-BYF_2.0$CaCl_2$ results are below that value during all the experiment. Moreover, Fig. 7b and 7c show the theoretical ettringite calculated according to reaction (1) considering the dissolution of both crystalline ye'elimite and anhydrite in B-BYF_REF and B-BYF_0.05TIPA pastes, and with the assumption of excess of the other chemical reactants. The experimental AFt in each paste has also been included here to facilitate the discussion. In these cases, both calculated values are almost coincident, and very close to the experimental ones, especially before ~7 h of hydration, supporting that in these pastes the followed pathway to form ettringite is close to equilibrium as expressed in reaction (1). In the TIPA-containing paste, after ~10 h, the difference between the experimental and the calculated AFt values increases with time. Consequently, the aluminate and sulfate bearing amorphous fraction of B-BYF is playing a role here, yielding to a slightly higher AFt precipitation. Consequently, it can be indirectly derived that TIPA has increased the solubility rate of aluminate- and sulfate-bearing amorphous phases. However, more research is needed to confirm/discard these findings, for instance, pore solution analysis.

However, to follow with this discussion, in the sample with $CaCl_2$, the molar ratio of crystalline C $\overline{S}$/C_4A_3 $\overline{S}$ is far from 2.0, Fig. 7a, indicating that there is a different pathway to form ettringite. A hypothesis is that the crystalline anhydrite that is dissolving yields to AFt following reaction (1), reacting with a fraction of crystalline ye'elimite. The AFt

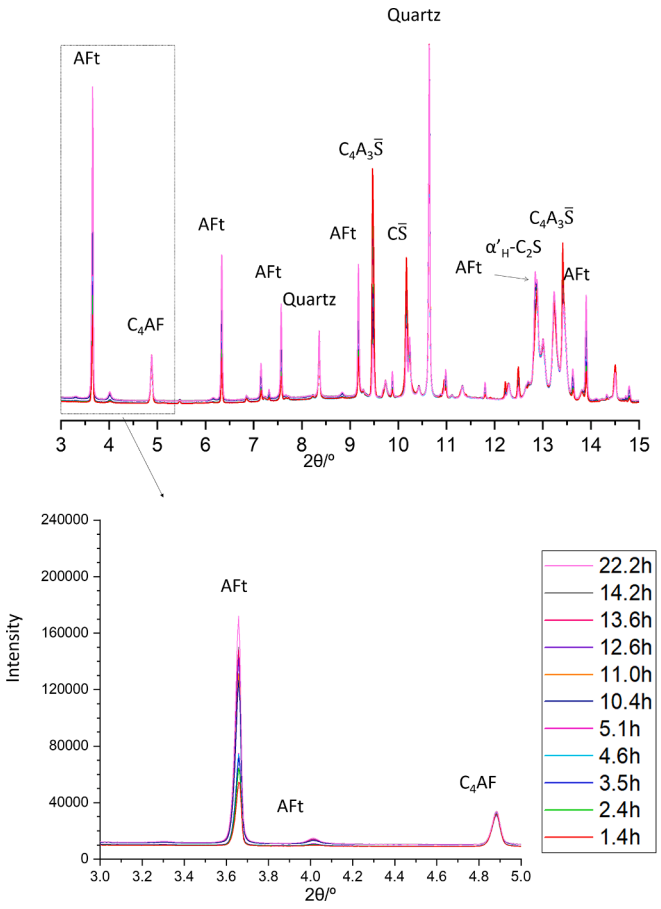

Fig. 4. Selected SXRPD raw patterns (λ = 0.62 Å) for B-BYF_2.0$CaCl_2$ paste. Bottom: enlarged low angle region.

calculated according to this hypothesis is shown in Fig. 7d. The *extra*-AFt formed is assumed to have precipitated from the dissolution of crystalline ye'elimite in a low sulfate environment. This behavior has been previously observed [45], in which a sample of pure ye'elimite with water yielded a mixture of ettringite and AFm-type phases. Consequently, assuming that there are two different pathways for AFt precipitation in the paste with $CaCl_2$, the amount of amorphous aluminate hydrates should be also higher than in the other pastes, as proved below.

Analyzing Figs. 6 and 7, a change on slope in the curves is observed at ~7 h. Consequently, pastes of B-BYF_REF and B-BYF_2.0$CaCl_2$ were also prepared *ex situ*, where the hydration was stopped at 4 h and 24 h, with the objective of obtaining information of phase assemblage before this change of hydration kinetics. Fig. 8 shows the deconvoluted ^{27}Al MAS-NMR spectra of B-BYF_REF and B-BYF_2.0$CaCl_2$, prepared by the same methodology as for the *in situ* SXRPD study, at 4 h and 24 h. These spectra show the Al^{IV} signals of ye'elimite at ~70 ppm, Al^{VI} of ettringite centered at ~13 ppm and the broader and less intense signals of Al^{VI} centered at ~12 ppm, corresponding to nanocrystalline-AH_3 and possibly to AFm-type phases [46].

Table 2 shows the relative population of Al^{IV} and Al^{VI} of each spectrum. The values given in Table 2 indicate that, in the presence of calcium chloride, the amount of amorphous aluminate hydrates is larger in comparison with the reference paste at 4 h and after 24 h. The nature of these aluminate hydrate cannot be unraveled from ^{27}Al MAS-NMR because the signals are very broad.

Fig. 9 gives the TGA curves for the three stopped pastes after 24 h. In this figure, the presence of the dehydroxylation of AH_3, centered at ~250 °C, is clearly present in B-BYF_REF and B-BYF_0.05TIPA, while in B-BYF_2.0$CaCl_2$, the signal is much broader and located at ~190 °C, which may be related to nanocrystalline AFm-phases [47]. The endotherm related to the dehydroxylation of AH_3 is usually broader in cements with low amount of anhydrite or gypsum as reported by [47], due to its small particle size or amorphous nature. Moreover, AFm-type phases also precipitate in systems with lower sulfate contents, giving signals located at ~190 °C, as described previously [48,49]. Consequently, these data are consistent with the hydration reaction deduced from SXRPD data and with ^{27}Al MAS-NMR, in which dissolution of anhydrite has been delayed by the presence of $CaCl_2$.

3.2. Calorimetric study

Fig. 10a displays the heat released by the three pastes determined by calorimetry during the first 24 h, with an enlarged inset for the heat evolved. Fig. 10b depicts the accumulated heat up to 24 h for the three samples, with the detailed values of accumulated heat at selected times of hydration as an inset. The three pastes evolved a heat flow higher than 50 mW/g during the first 10 min of hydration, mainly due to the wetting of the sample and first dissolution of ye'elimite, followed by a fast decrease of heat. These first signals are almost coincident for all the samples, independently on the admixture. After this, the induction period starts in which the rate of dissolution of ye'elimite and anhydrite falls slowly and the formation of ettringite and amorphous hydrates continues [50]. In this stage, there is a small signal at ~3 h in REF and TIPA samples, that disappears in the paste with $CaCl_2$. This is mainly due to the dissolution of anhydrite which is partially delayed by the presence of calcium chloride due to the common ion effect. Then the three pastes show an induction period that ends at 7.4, 7.2 and 6.4 h, for REF, TIPA and $CaCl_2$ pastes, respectively (determined by the interception of two lines as shown in the inset of Fig. 10a). These values should be compared with the data presented in Figs. 6 and 7. Although the in-situ SXRPD data have been obtained with quartz as internal standard and may present slightly accelerated hydration reactions due to the well-known filler effect [51,52], the time values are almost coincident with the change of slope (of the curves) for dissolution and precipitation phenomena, shown in Figs. 6 and 7. Consequently, the most important heat flow signals occur from the massive dissolution of ye'elimite and anhydrite, followed by a massive precipitation of ettringite [15]. On the one hand, the addition of TIPA produced an almost negligible effect on the heat evolved. On the other hand, $CaCl_2$ acted as an accelerator, decreasing the induction period and narrowing the heat signals associated to ettringite formation. This type of acceleration has been previously described in similar BYF systems by reducing the w/c ratio [49]. These findings also agree with the results from the *in situ* SXRPD study, and support the reaction pathway for ettringite formation explained before.

3.3. Rheological study

Fig. 11 shows the flow curves of the three pastes measured just after 8 min from the hydration initiation. The amount and type of accelerator and the hydration time will affect the rheological behavior of the pastes. All these pastes follow the Herschel-Bulkley model, with a value of the corresponding index, higher than 1 (viz. 1.26, 1.23 and 1.24, for B-BYF_REF, B-BYF_0.05TIPA and B-BYF_2.0$CaCl_2$, respectively, from the down-curve) indicating a slight shear thickening behavior. On the one hand, the addition of 0.05 wt% of TIPA decreased the shear stress, and consequently the viscosity, of the B-BYF paste at any shear rate (f.i. 323 mPas and 118 mPas at 100 s^{-1}, without and with TIPA, respectively, from the down-curve). It has been published [53–57] that the viscosity depends not only on the alkanolamine kind, dosage, cement type, but also on the hydration time. The improved fluidity (lower viscosity) of mortars with TIPA at the very beginning of the hydration may be explained [56] by the reduction of cement agglomerates through the modification of interparticle forces. The admixture may be in the interstitial paste solution, and consequently, not adsorbed onto the cement particles surface [58], or may interact with the cement grains [57]. On the other hand, the presence of $CaCl_2$ increased both viscosity

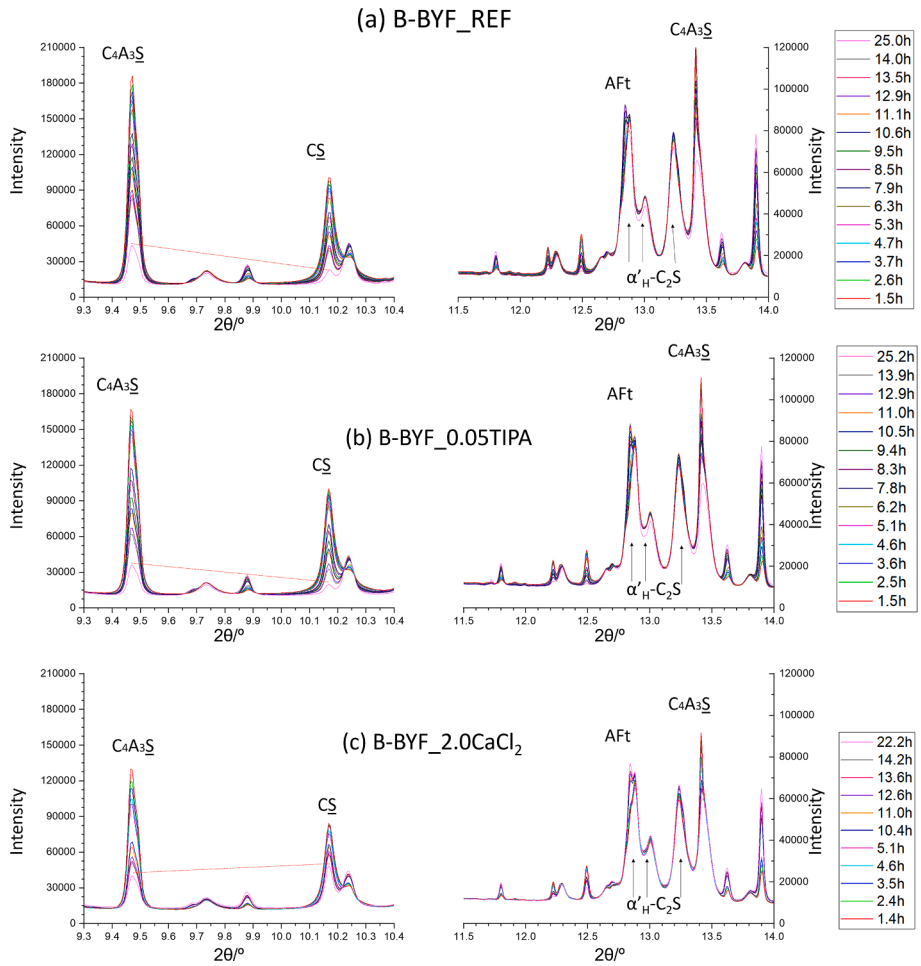

Fig. 5. Selected ranges of SXRPD raw patterns (λ = 0.62 Å) collected within the first ~24 h of hydration for (a) B-BYF_REF, (b) B-BYF_0.05TIPA and (c) B-BYF_2.0$CaCl_2$ pastes.

(viz. 446 mPas at 100 s^{-1}, from the down-curve) and the thixotropic cycle (10^4 Pa/s for the paste with $CaCl_2$, but almost negligible for the other two pastes) referred to the reference paste. It has been described [44,59] that the addition of calcium chloride in PC pastes reduces the calcium sulfate solubility, and consequently the sulfate anion concentration in the aqueous phase decreases. As the adsorption of polycarboxylate-based SP onto sulfate and PC particles (e.g. C_3A) is competitive, this would favor the adsorption onto the latter, increasing fluidity (and reducing viscosity). However, by increasing the $CaCl_2$ content above a certain amount (viz. 1.1 %*bwc* for PC with w/c = 0.3 [44]), the effect of the ionic strength may gain prominence with the consequent decrease in fluidity. Thus, the increase in viscosity and thixotropic cycle here may be attributed to both the increase in ionic strength in the paste (as a relatively high amount of $CaCl_2$ was added), and the higher precipitation of AFt from very early ages. Actually, at 0.8 h of hydration, higher contents of crystalline AFt were quantified for B-BYF_2.0$CaCl_2$ than for the other two pastes even at longer times, f.i. 1.5 h, Tables S1 to S3 and Fig. 6.

3.4. Mechanical strengths

The mechanical strength values (compression) of the mortars of B-BYF without and with the addition of the two admixtures after 24 h of hydration were 16.6(2), 28(3) and 30(1) MPa, for B-BYF_REF, B-BYF_0.05TIPA and B-BYF_2.0$CaCl_2$, respectively. The increase of early mechanical strengths is firmly established. Although, the direct correlation between results obtained from pastes with those obtained from mortars is not straightforward and should be taken with caution, a discussion is included here. On the one hand, the lower viscosity of the paste with TIPA at very early ages may have yielded to a more homogeneous mortar and consequently, to higher mechanical strengths, jointly to the fact that slightly higher AFt contents were quantified for the TIPA paste than for the REF one (viz. 28.6 and 31.1 wt%, respectively, Tables S1 and S2). On the other hand, the addition of $CaCl_2$, has caused a slightly larger degree of hydration of ye'elimite yielding a larger amount of amorphous hydrated phases. The large 1-day compressive strength value for the $CaCl_2$ containing sample seems to indicate that the amorphous calcium aluminate hydrated phase has high binding properties. However, more studies are needed to firmly establish this point. Finally, it should be noted that the three binders show very similar cumulative heats at 24 h which indicated that the released heat is not a good descriptor for predicting the mechanical strengths.

4. General discussion

The selective effect of two different admixtures, TIPA and $CaCl_2$, on the hydration of an active B-BYF cement has been studied. Tables S1–S3 give the full phase assemblage obtained from the SXRPD study, including the total ACn content, which comprises the amount of amorphous/nanocrystalline hydrated phases and the weight percentage of free water, i.e. non-chemically combined water, at each hydration time. Considering the results presented in Figs. 6 and 7, it can be stated that the reaction pathway of REF and TIPA pastes goes through reaction (1). Consequently, Fig. 12 shows the calculated amount of amorphous/

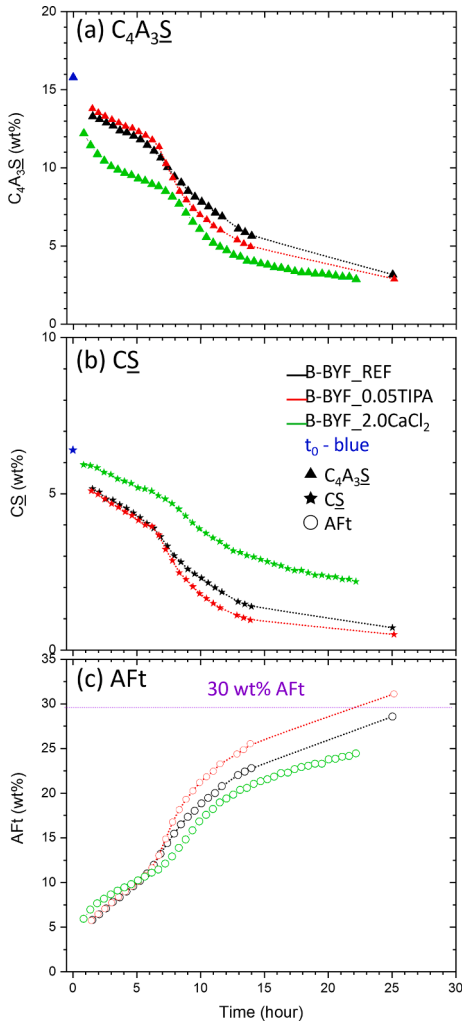

Fig. 6. (a) Ye'elimite, (b) anhydrite and (c) ettringite phase evolutions with time obtained from RQPA of *in situ* SXRPD study of B-BYF_REF (black), B-BYF_0.05TIPA (red) and B-BYF_2.0CaCl$_2$ (green). In (c) the purple dashed line indicates the maximum amount of AFt, considering Al_2O_3 as the limiting reactant (excluding the Al_2O_3 in ferrite and gehlenite). *Symbols in blue are the amount of each phase in the anhydrous cement renormalized with the nominal added water. (For interpretation of the references to colour in this figure legend, the reader is referred to the web version of this article.)

nanocrystalline $AH_3{\cdot}5H$ (ACn_{calc}) and the calculated amount of non-combined water, FW_{calc}, considering the stoichiometry of reaction (1). These values match fairly well with the total ACn content experimentally obtained, also included in Fig. 12. Furthermore, the value of FW experimentally determined by TGA by stopping the pastes after 24 h of hydration, also matches the calculated values. This agreement shows the robustness of the methodologies.

Moreover, the paste with $CaCl_2$ has presented a different hydration pathway. In this paste, the fraction of dissolved anhydrite was lower, probably due to a decrease in its solubility due to the common ion effect. The dissolved anhydrite fraction reacted with ye'elimite to give ettringite and $AH_3{\cdot}5H$ according to reaction (1). In addition, it was observed that another fraction of ye'elimite dissolved and gave rise to ettringite, but without the presence of calcium sulfate. Winnefeld & Lothenbach [60], through thermodynamic calculations of the stable hydrate assemblage in calcium sulfoaluminate cements, predicted reaction (5), where ye'elimite dissolved to give a mixture of ettringite, calcium aluminate decahydrate and aluminum hydroxide gel. The calculations carried out here assumed that the aluminum hydroxide gel shows the same water content as that given in reaction (1).

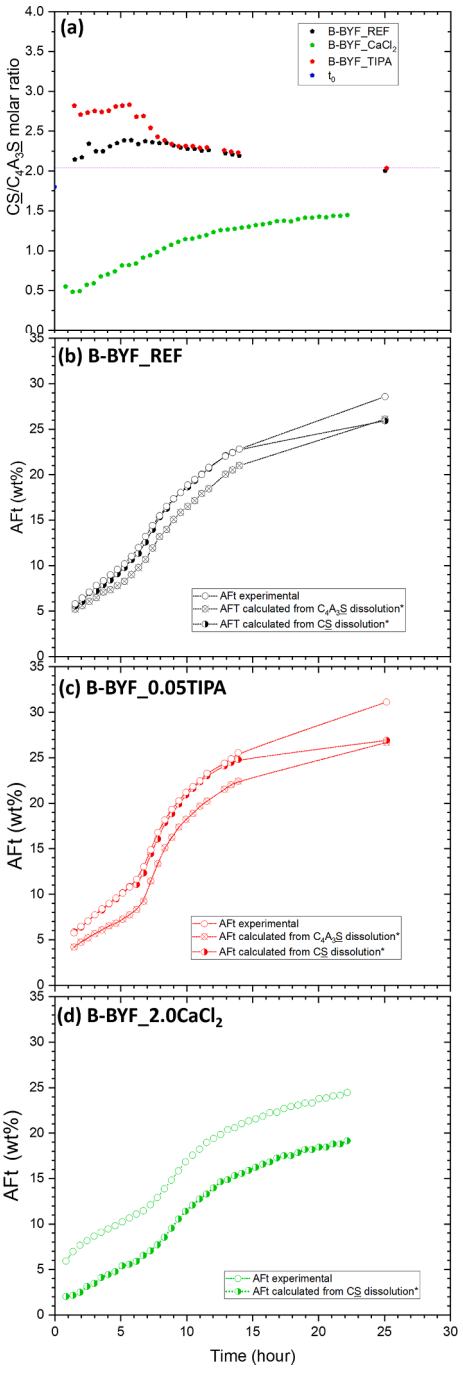

Fig. 7. (a) Crystalline consumed anhydrite/ye'elimite molar ratio; (b) AFt in B-BYF_REF, (c) AFt in B-BYF_TIPA and (d) AFt in B-BYF_2.0CaCl$_2$. *For the AFt calculations according to reaction (1), excess of the other chemical reactants has been assumed.

$$C_4A_3\,\overline{S} + 104H \rightarrow C_6A\,\overline{S}_3H_{32} + 6CAH_{10} + 2AH_3{\cdot}5H \quad (5)$$

Thus, the amount of water consumed and the quantity of CAH_{10} and $AH_3{\cdot}5H$ formed have been calculated according to the stoichiometry of reaction (5); the two latter phases were considered amorphous, as no diffraction signals have been observed in the SXRPD study. Fig. 12c shows the calculated uncombined water content (free water) and the calculated amorphous content (the sum of $AH_3{\cdot}5H$ according to reaction (1), and CAH_{10} and $AH_3{\cdot}5H$ according to reaction (5)). As can be seen, again the results of the total ACn obtained with the SXRPD study agree quite well with the calculated data. In addition, the 1-day free water obtained with an independent method such as TGA, coincides well,

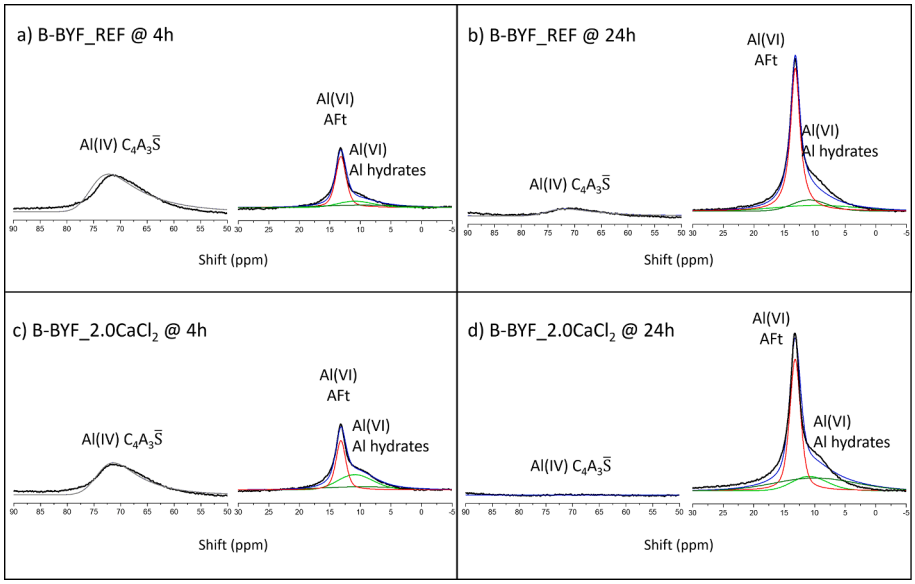

Fig. 8. ^{27}Al MAS-NMR spectra for (a) B-BYF_REF and (c) B-BYF_2.0$CaCl_2$ after 4 h of hydration; (b) B-BYF_REF and (d) B-BYF_2.0$CaCl_2$ at 24 h of hydration. The deconvoluted signals are included: blue for cumulative fit peak, grey for Al^{IV} site of yéelimite, red for Al^{VI} site of ettringite, dark and light green for Al^{VI} site of amorphous aluminate hydrates. (For interpretation of the references to colour in this figure legend, the reader is referred to the web version of this article.)

Table 2
Relative population distribution of Al^{IV} of $C_4A_3\bar{S}$, Al^{VI} of AFt, Al^{VI} sites of aluminate hydrates of B-BYF_REF and B-BYF_2.0$CaCl_2$ at both 4 and 24 h of hydration..

Paste	Al^{IV} $C_4A_3\bar{S}$ / %	Al^{VI} AFt/ %	Al^{VI} aluminate hydrates/ %
B-BYF_REF @ 4 h	66.4	21.7	12.0
B-BYF_2.0$CaCl_2$ @ 4 h	54.8	19.5	25.7
B-BYF_REF @ 24 h	12.1	64.0	23.9
B-BYF_2.0$CaCl_2$ @ 24 h	0.0	58.4	41.6

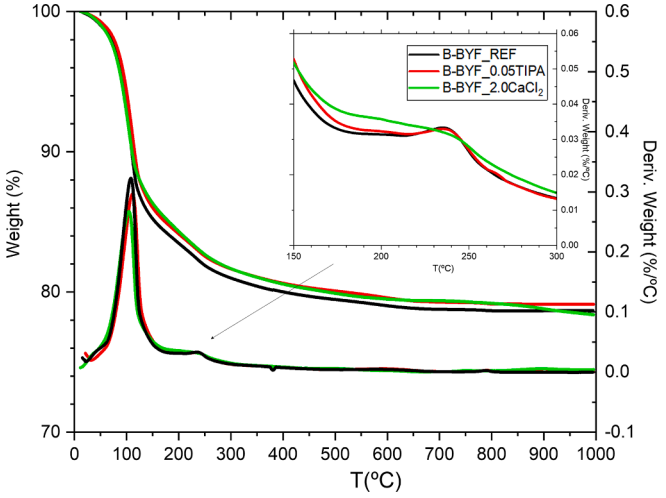

Fig. 9. TGA and derivative TGA curves for the three pastes stopped after 24 h of hydration. The inset is the enlarged range of the derivative TGA from 150 to 300 °C.

which indicates that the reaction pathway proposed is plausible.

^{27}Al-NMR data has been performed to corroborate the findings from the in-situ SXRPD study. As discussed just above, the presence of $CaCl_2$, has modified the pathway of ye'elimite hydration. The ^{27}Al-NMR signal of ettringite (~13 ppm) for all samples shows a narrow line width, due to its ordered crystalline nature, Fig. 8. At the same time, the signals related to nanocrystalline aluminum hydroxide or other distorted/disordered aluminate hydrates are centered at ~12 ppm. The analysis of these spectra, Table 2, confirms that the amount of aluminate hydrates is larger in the sample with chloride. The chemical nature of these amorphous, or nanocrystalline, aluminate hydrates can not be directly determined due to the broadness of the ^{27}Al-NMR signals. However, supported by the calculations discussed just above, and given in Fig. 12, it can be speculated that the amorphous/nanocrystalline phases in REF sample presents a stoichiometry close to hydrated aluminum hydroxide, and that of $CaCl_2$ should be close to a mixture of nanocrystalline CAH_{10} and hydrated aluminum hydroxide.

5. Conclusions

In this study the effect of TIPA and $CaCl_2$ on early hydration of a B-BYF cement is presented. The *in situ* SXRPD study has enabled to unravel the particular effect of each admixture on the kinetic of hydration. On the one hand, before the induction period finishes, the presence of 0.05 %*bwc* of TIPA had almost no effect on the dissolution kinetic of both ye'elimite and anhydrite and consequently, the precipitation of ettringite. After this, TIPA mobilized a fraction of the amorphous aluminate and sulfates to yield a slightly higher precipitation of AFt. In any case, the stoichiometry of this paste followed the well-known pathway reaction of 1.0 mol ettringite formation from 1.0 and 2.0 mol of ye'elimite and calcium sulfate, respectively, reaction (1). On the other hand, the addition of 2.0 %*bwc* $CaCl_2$ has selectively boosted the dissolution kinetic of ye'elimite with a degree of hydration (DoH) of this phase of 46% in this paste, meanwhile its DoH was 33 and 28% for the reference and the TIPA pastes, respectively. At the same time, the dissolution of anhydrite has been slightly delayed, and consequently, the formation of ettringite seems to follow two coincident reaction pathways: i) the consumption of calcium sulfate, following reaction (1), and ii) the *extra*-ye'elimite dissolved that yielded a mixture of AFt and amorphous aluminate hydrate. Finally, it was shown that neither C_4AF nor α'_H-C_2S reactivities were affected by the addition of these amounts of TIPA or $CaCl_2$, within the first 24 h.

The calorimetric study confirmed the acceleration effect of $CaCl_2$, by shortening the end of the induction period by ~1 h when compared to

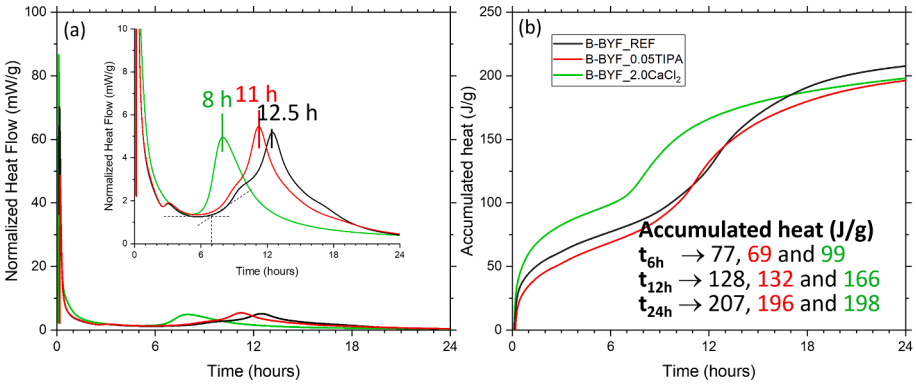

Fig. 10. Calorimetric curves up to 24 h for all B-BYF pastes with w/c = 0.40 and 0.4 wt% of SP with different admixtures. (a) Heat flow traces normalized to the amount of cement. (b) Cumulative heats. Inset in (a): enlarged view for better visualization.

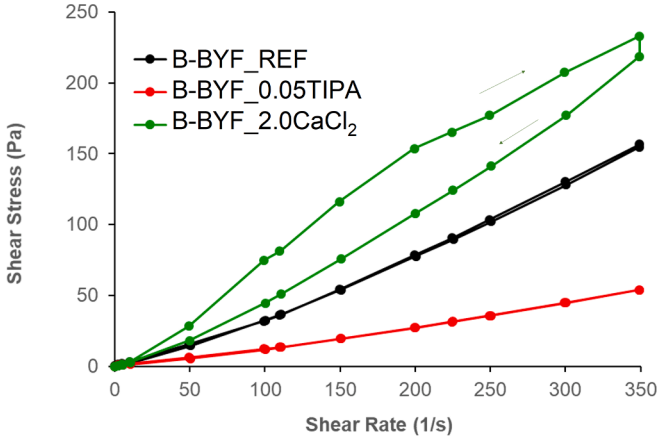

Fig. 11. Flow curves of the three studied pastes.

the reference paste. The effect of TIPA in the heat evolved was almost negligible.

The rheological study showed that both admixtures have an important impact on the viscosity of the paste within the first minutes of hydration; TIPA reduces it mainly due to the reduction of cements agglomerates, while $CaCl_2$ increases it, likely due to the higher ionic strength jointly with the increased AFt content.

Finally, the effect of the addition of these accelerators in the early compressive strengths has been positive, since in both mortars, the one-day mechanical strengths outperform that of the reference, with an increase of 169% and 181%, for mortars with 0.05 %*bwc* of TIPA and 2.0 %*bwc* of $CaCl_2$, respectively. According to the results obtained, and taken with caution because the correlation of results obtained with pastes and those with mortars is not straightforward, these enhancements may be due to i) the lower viscosity of the fresh paste and the slightly higher amount of AFt in the paste with TIPA and ii) due to the slightly larger precipitation of AFt in the first hours of hydration jointly with a higher amount of amorphous phases in the paste with $CaCl_2$.

CRediT authorship contribution statement

Raquel Pérez-Bravo: Investigation, Methodology, Writing – review & editing. **Alejandro Morales-Cantero:** Investigation, Methodology, Writing – review & editing. **Ana Cuesta:** Investigation, Methodology, Writing – review & editing. **Miguel A.G. Aranda:** Investigation, Writing – review & editing. **Isabel Santacruz:** Investigation, Funding acquisition, Supervision, Writing – review & editing. **Angeles G. De la Torre:** Conceptualization, Funding acquisition, Supervision, Writing – original draft, Writing – review & editing.

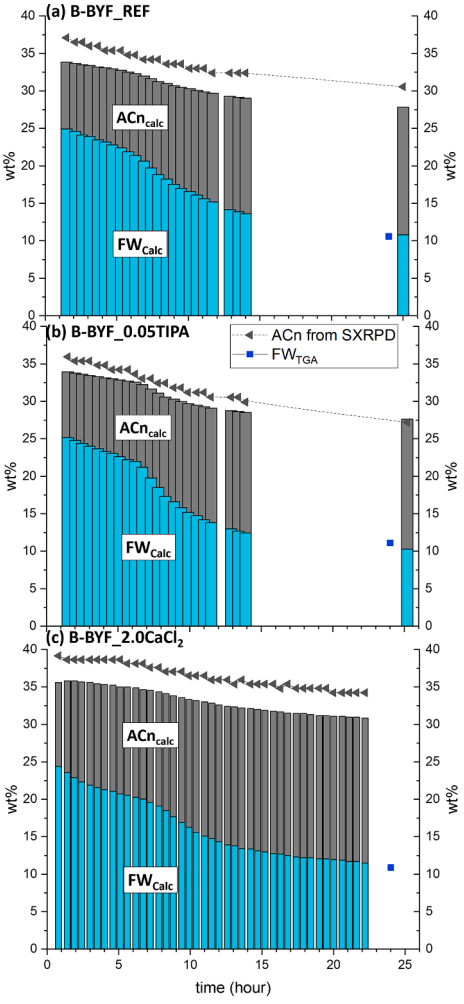

Fig. 12. ACn total content obtained by SXRPD study. Calculated amorphous/nanocrystalline hydrated phases (ACn_{calc}) and non-chemically bounded water, free water, FW_{calc}, according to reactions (1) in (a) and (b) and reactions (1) and (5) in (c), see text. Blue squares stand for the free water calculated by TGA at 24 h. (For interpretation of the references to colour in this figure legend, the reader is referred to the web version of this article.)

Declaration of Competing Interest

The authors declare that they have no known competing financial interests or personal relationships that could have appeared to influence

the work reported in this paper.

Data availability

The SXRPD raw data are freely deposited on Zenodo at 10.5281/zenodo.7330339

Acknowledgements

P18-RT-720 from the Andalusian regional government and PID2019-104378RJ-I00 from the Spanish government are gratefully acknowledged. ALBA synchrotron is acknowledged for providing with beamtime at MSPD beamline. Funding for open access charge: Universidad de Málaga / CBUA.

Data availability

The SXRPD raw data are freely deposited on Zenodo at 10.5281/zenodo.7330339.

Appendix A. Supplementary data

Supplementary information includes Tables S1 to S3 with the RQPA results, including the ACn contents, all the patterns collected of the three pastes during the first 24 hours. Fig. S1 shows selected Rietveld plots. Supplementary data to this article can be found online at https://doi.org/10.1016/j.conbuildmat.2023.130765.

References

[1] W.B.C. for Sustainable Development, Cement Sustainability Initiative. Cement industry energy and CO2 performance "getting the numbers right, Cem. Sustain. Initiat. (2009).
[2] D. Hodgson, T. Vass, P. Hugues, Cement, IEA, Paris, 2022.
[3] G. Habert, S.A. Miller, V.M. John, J.L. Provis, A. Favier, A. Horvath, K.L. Scrivener, Environmental impacts and decarbonization strategies in the cement and concrete industries, Nat. Rev. Earth Environ. 1 (2020) 559–573, https://doi.org/10.1038/s43017-020-0093-3.
[4] E. Gartner, H. Hirao, A review of alternative approaches to the reduction of CO2 emissions associated with the manufacture of the binder phase in concrete, Cem. Concr. Res. 78 (2015) 126–142, https://doi.org/10.1016/J.CEMCONRES.2015.04.012.
[5] M.A.G. Aranda, A.G. De la Torre, Sulfoaluminate cement, in: F. Pacheco-Torgal, S. Jalali, J. Labrincha (Eds.), Eco-Efficient Concr., 2013: pp. 488–522. https://doi.org/10.1533/9780857098993.4.488.
[6] V. Morin, P. Termkhajornkit, B. Huet, G. Pham, Impact of quantity of anhydrite, water to binder ratio, fineness on kinetics and phase assemblage of belite-ye'elimite-ferrite cement, Cem. Concr. Res. 99 (2017) 8–17, https://doi.org/10.1016/j.cemconres.2017.04.014.
[7] G. Alvarez-Pinazo, I. Santacruz, M.A.G. Aranda, A.G. De la Torre, Hydration of belite–ye'elimite–ferrite cements with different calcium sulfate sources, Adv. Cem. Res. 28 (2016) 529–543, https://doi.org/10.1680/jadcr.16.00030.
[8] A. Cuesta, A.G. De la Torre, I. Santacruz, P. Trtik, J.C. Da Silva, A. Diaz, M. Holler, M.A.G. Aranda, Chemistry and mass density of aluminum hydroxide gel in eco-cements by ptychographic X-ray computed tomography, J. Phys. Chem. C. 121 (2017) 3044–3054, https://doi.org/10.1021/acs.jpcc.6b10048.
[9] L.E. Burris, K.E. Kurtis, Influence of set retarding admixtures on calcium sulfoaluminate cement hydration and property development, Cem. Concr. Res. 104 (2018) 105–113, https://doi.org/10.1016/J.CEMCONRES.2017.11.005.
[10] M. Zajac, J. Skocek, F. Bullerjahn, M. Ben Haha, Effect of retarders on the early hydration of calcium-sulpho-aluminate (CSA) type cements, Cem. Concr. Res. 84 (2016) 62–75, https://doi.org/10.1016/j.cemconres.2016.02.014.
[11] J. Péra, J. Ambroise, New applications of calcium sulfoaluminate cement, Cem. Concr. Res. 34 (2004) 671–676, https://doi.org/10.1016/j.cemconres.2003.10.019.
[12] R. Belhadi, A. Govin, P. Grosseau, Influence of polycarboxylate superplasticizer, citric acid and their combination on the hydration and workability of calcium sulfoaluminate cement, Cem. Concr. Res. 147 (2021), 106513, https://doi.org/10.1016/J.CEMCONRES.2021.106513.
[13] G. Zhang, G. Li, Y. Li, Effects of superplasticizers and retarders on the fluidity and strength of sulphoaluminate cement, Constr. Build. Mater. 126 (2016) 44–54, https://doi.org/10.1016/j.conbuildmat.2016.09.019.
[14] H. Tayyab Adnan, A. Kienzle, R.J. Thomas, Engineering properties and setting time of belitic calcium sulfoaluminate (BCSA) cement concrete, Constr. Build. Mater. 352 (2022), 128979, https://doi.org/10.1016/j.conbuildmat.2022.128979.
[15] F. Bullerjahn, M. Zajac, J. Skocek, M. Ben Haha, The role of boron during the early hydration of belite ye'elimite ferrite cements, Constr. Build. Mater. 215 (2019) 252–263, https://doi.org/10.1016/J.CONBUILDMAT.2019.04.176.
[16] G. Alvarez-Pinazo, I. Santacruz, L. León-Reina, M.A.G. Aranda, A.G. De la Torre, Hydration reactions and mechanical strength developments of iron-rich sulfobelite eco-cements, Ind. Eng. Chem. Res. 52 (2013) 16606–16614, https://doi.org/10.1021/ie402484e.
[17] E. Gartner, G. Li, High belite-containing sulfoaluminous clinker, method for the production and the use thereof for preparing hydraulic binders., 04-51586 (publication 2873366), 2006.
[18] A. Cuesta, E.R. Losilla, M.A.G. Aranda, J. Sanz, A.G. De la Torre, Reactive belite stabilization mechanisms by boron-bearing dopants, Cem. Concr. Res. 42 (2012) 598–606, https://doi.org/10.1016/j.cemconres.2012.01.006.
[19] Y. Hu, W. Li, S. Ma, Q. Wang, H. Zou, X. Shen, The composition and performance of alite-ye'elimite clinker produced at 1300 °C, Cem. Concr. Res. 107 (2018) 41–48, https://doi.org/10.1016/j.cemconres.2018.02.009.
[20] J.D. Zea-Garcia, A.G. De, la, Torre, M.A.G. Aranda, I. Santacruz, Processing and characterisation of standard and doped alite-belite-ye'elimite ecocement pastes and mortars, Cem. Concr. Res. 127 (2020), 105911, https://doi.org/10.1016/j.cemconres.2019.105911.
[21] D. Londono-Zuluaga, J.I. Tobón, M.A.G. Aranda, I. Santacruz, A.G. De la Torre, Clinkering and hydration of belite-alite-ye'elimite cement, Cem. Concr. Compos. 80 (2017) 333–341.
[22] T. Dorn, O. Blask, D. Stephan, Acceleration of cement hydration – A review of the working mechanisms, effects on setting time, and compressive strength development of accelerating admixtures, Constr. Build. Mater. 323 (2022), 126554, https://doi.org/10.1016/j.conbuildmat.2022.126554.
[23] J. Bensted, P. Barnes, Structure and Performance of Cements, Spon Press, 2002.
[24] G. Li, J. Zhang, Z. Song, C. Shi, A. Zhang, Improvement of workability and early strength of calcium sulphoaluminate cement at various temperature by chemical admixtures, Constr. Build. Mater. 160 (2018) 427–439, https://doi.org/10.1016/J.CONBUILDMAT.2017.11.076.
[25] Z. Xu, W. Li, J. Sun, Y. Hu, K. Xu, S. Ma, X. Shen, Research on cement hydration and hardening with different alkanolamines, Constr. Build. Mater. 141 (2017) 296–306, https://doi.org/10.1016/j.conbuildmat.2017.03.010.
[26] E. Gartner, D. Myers, Influence of tertiary alkanolamines on portland cement hydration, J. Am. Ceram. Soc. 76 (1993) 1521–1530, https://doi.org/10.1111/j.1151-2916.1993.tb03934.x.
[27] G. Alvarez-Pinazo, A. Cuesta, M. García-Maté, I. Santacruz, E.R. Losilla, A.G. De la Torre, L. León-Reina, M.A.G. Aranda, Rietveld quantitative phase analysis of Yeelimite-containing cements, Cem. Concr. Res. 42 (2012) 960–971, https://doi.org/10.1016/j.cemconres.2012.03.018.
[28] R. Pérez-Bravo, A. Morales-Cantero, M. Bruscolini, M.A.G. Aranda, I. Santacruz, A. G. De la Torre, Effect of boron and water-to-cement ratio on the performances of laboratory prepared belite-ye'elimite-ferrite (BYF) cements, Materials (Basel). 14 (2021) 4862, https://doi.org/10.3390/ma14174862.
[29] A.G. De la Torre, S. Bruque, M.A.G. Aranda, Rietveld quantitative amorphous content analysis, J. Appl. Crystallogr. 34 (2001) 196–202, https://doi.org/10.1107/S0021889801002485.
[30] F. Fauth, I. Peral, C. Popescu, M. Knapp, The new material science powder diffraction beamline at ALBA synchrotron, Cambridge Univ. Press 28 (S2) (2013) S360–S370.
[31] B.H. Toby, R.B. Von Dreele, IUCr, GSAS-II: the genesis of a modern open-source all purpose crystallography software package, Urn 46 (2013) 544–549, https://doi.org/10.1107/S0021889813003531. Issn:0021-8898.
[32] A. Morales-Cantero, A. Cuesta, A.G. De la Torre, I. Santacruz, O. Mazanec, P. Borralleras, K.S. Weldert, D. Gastaldi, F. Canonico, M.A.G. Aranda, C-S-H seeding activation of Portland and Belite Cements: an enlightening in situ synchrotron powder diffraction study, Cem. Concr. Res. 161 (2022), 106946, https://doi.org/10.1016/j.cemconres.2022.106946.
[33] A.G. De la Torre, I. Santacruz, A. Cuesta, L. León-Reina, M.A.G. Aranda, Diffraction and crystallography applied to anhydrous cements, in: H. Pöllmann (Ed.), Cem. Mater., De Gruyter, 2017, pp. 3–29.
[34] M.A.G. Aranda, A. Cuesta, A.G. De la Torre, I. Santacruz, L. León-Reina, Diffraction and crystallography applied to hydrating cements, 2017. https://doi.org/10.1515/9783110473728-003.
[35] L. Wadsö, Operational issues in isothermal calorimetry, Cem. Concr. Res. 40 (2010) 1129–1137, https://doi.org/10.1016/j.cemconres.2010.03.017.
[36] A. Quennoz, K.L. Scrivener, Interactions between alite and C3A-gypsum hydrations in model cements, Cem. Concr. Res. 44 (2013) 46–54, https://doi.org/10.1016/j.cemconres.2012.10.018.
[37] R. Snellings, J. Chwast, Ö. Cizer, N. De Belie, Y. Dhandapani, P. Durdzinski, J. Elsen, J. Haufe, D. Hooton, C. Patapy, M. Santhanam, K. Scrivener, D. Snoeck, L. Steger, S. Tongbo, A. Vollpracht, F. Winnefeld, B. Lothenbach, Report of TC 238-SCM: hydration stoppage methods for phase assemblage studies of blended cements—results of a round robin test, Mater. Struct. Constr. 51 (2018), https://doi.org/10.1617/s11527-018-1237-5.
[38] D. Massiot, F. Fayon, M. Capron, I. King, S. Le Calvé, B. Alonso, J.-O. Durand, B. Bujoli, Z. Gan, G. Hoatson, Modelling one- and two-dimensional solid-state NMR spectra, Magn. Reson. Chem. 40 (2002) 70–76, https://doi.org/10.1002/mrc.984.
[39] J.B. d'Espinose de Lacaillerie, C. Fretigny, D. Massiot, MAS NMR spectra of quadrupolar nuclei in disordered solids: The Czjzek model, J. Magn. Reson. 192 (2008) 244–251, https://doi.org/10.1016/J.JMR.2008.03.001.
[40] M. García-Maté, A.G. De la Torre, L. León-Reina, E.R. Losilla, M.A.G. Aranda, I. Santacruz, Effect of calcium sulfate source on the hydration of calcium

sulfoaluminate eco-cement, Cem. Concr. Compos. 55 (2015) 53–61, https://doi.org/10.1016/j.cemconcomp.2014.08.003.
[41] B. Lothenbach, P. Durdzinski, K. De Weerdt, Thermogravimetric analysis, in: K. Scrivener, R. Snellings, B. Lothenbach (Eds.), A Pract. Guid. to Microstruct. Anal. Cem. Mater, CRC Press, U.S.A, 2016, pp. 177–211.
[42] T. Duvallet, Y. Zhou, K.R. Henke, T.L. Robl, R. Andrews, Effects of ferrite concentration on synthesis, hydration and mechanical properties of alite-calcium sulfoaluminate-ferrite cements, J. Sustain. Cem. Mater. 6 (2) (2017) 85–110.
[43] F. Winnefeld, B. Lothenbach, Hydration of calcium sulfoaluminate cements — Experimental findings and thermodynamic modelling, Cem. Concr. Res. 40 (8) (2010) 1239–1247.
[44] K. Yamada, S. Ogawa, S. Hanehara, Controlling of the adsorption and dispersing force of polycarboxylate-type superplasticizer by sulfate ion concentration in aqueous phase, Cem. Concr. Res. 31 (2001) 375–383, https://doi.org/10.1016/S0008-8846(00)00503-2.
[45] A. Cuesta, G. Alvarez-Pinazo, S.G. Sanfélix, I. Peral, M.A.G. Aranda, A.G. De la Torre, Hydration mechanisms of two polymorphs of synthetic ye'elimite, Cem. Concr. Res. 63 (2014) 127–136, https://doi.org/10.1016/j.cemconres.2014.05.010.
[46] D. Gastaldi, G. Paul, L. Marchese, S. Irico, E. Boccaleri, S. Mutke, L. Buzzi, F. Canonico, Hydration products in sulfoaluminate cements: evaluation of amorphous phases by XRD/solid-state NMR, Cem. Concr. Res. 90 (2016) 162–173, https://doi.org/10.1016/j.cemconres.2016.05.014.
[47] F. Song, Z. Yu, F. Yang, Y. Lu, Y. Liu, Microstructure of amorphous aluminum hydroxide in belite-calcium sulfoaluminate cement, Cem. Concr. Res. 71 (2015) 1–6, https://doi.org/10.1016/j.cemconres.2015.01.013.
[48] D. Su, Q. Li, Y. Guo, G. Yue, L. Wang, Effect of residual $CaSO_4$ in clinker on properties of high belite sulfoaluminate cement based on solid wastes, Materials (Basel). 13 (2) (2020) 429.
[49] G.Y. Koga, B. Albert, R.P. Nogueira, On the hydration of Belite-Ye'elimite-Ferrite (BYF) cement pastes: Effect of the water-to-cement ratio and presence of fly ash, Cem. Concr. Res. 137 (2020), 106215, https://doi.org/10.1016/j.cemconres.2020.106215.
[50] F. Bullerjahn, E. Boehm-Courjault, M. Zajac, M. Ben Haha, K.L. Scrivener, Hydration reactions and stages of clinker composed mainly of stoichiometric ye'elimite, Cem. Concr. Res. 116 (2019) 120–133, https://doi.org/10.1016/J.CEMCONRES.2018.10.023.
[51] E. Berodier, K. Scrivener, G. Scherer, Understanding the filler effect on the nucleation and growth of C-S-H, J. Am. Ceram. Soc. 97 (12) (2014) 3764–3773.
[52] A. Morales-Cantero, A. Cuesta, I. Santacruz, M.A.G. Aranda, A.G. De la Torre, Phase-selective degree of hydration at setting: An in situ synchrotron diffraction study, Constr. Build. Mater. 328 (2022), 127117, https://doi.org/10.1016/J.CONBUILDMAT.2022.127117.
[53] V. Kobya, Y. Kaya, A. Mardani-Aghabaglou, Effect of amine and glycol-based grinding aids utilization rate on grinding efficiency and rheological properties of cementitious systems, J. Build. Eng. 47 (2022) 103917.
[54] J.J. Assaad, C.A. Issa, Effect of clinker grinding aids on flow of cement-based materials, Cem. Concr. Res. 63 (2014) 1–11, https://doi.org/10.1016/J.CEMCONRES.2014.04.006.
[55] I. Aiad, A.A. Mohammed, S.A. Abo-El-Enein, Rheological properties of cement pastes admixed with some alkanolamines, Cem. Concr. Res. 33 (2003) 9–13, https://doi.org/10.1016/S0008-8846(02)00911-0.
[56] M. Katsioti, P.E. Tsakiridis, P. Giannatos, Z. Tsibouki, J. Marinos, Characterization of various cement grinding aids and their impact on grindability and cement performance, Constr. Build. Mater. 23 (2009) 1954–1959, https://doi.org/10.1016/J.CONBUILDMAT.2008.09.003.
[57] J.J. Assaad, C.A. Issa, Rheological properties of cement pastes containing amine- and glycol-based grinding aids, Adv. Cem. Res. 27 (2015) 28–41, https://doi.org/10.1680/adcr.13.00066.
[58] J.P. Perez, A. Nonat, S. Pourchet, S. Garrault, M. Mosquet, C. Canevet, Why TIPA leads to an increase in the mechanical properties of mortars whereas TEA does not, ACI Symp. Publ. 217 (2003) 583–594.
[59] A. Griesser, Cement-Superplasticizer Interactions at Ambient Temperatures, ETH zürich Swiss Federal, Institute of Technology (2002), https://doi.org/10.3929/ethz-a-004470198.
[60] F. Winnefeld, B. Lothenbach, Phase equilibria in the system $Ca_4Al_6O_{12}SO_4$ – Ca_2SiO_4 – $CaSO_4$ – H_2O referring to the hydration of calcium sulfoaluminate cements, RILEM Tech. Lett. 1 (2016) 10, https://doi.org/10.21809/rilemtechlett.v1.5.